Cell

The ER UDPase ENTPD5 Promotes Protein N-Glycosylation, the Warburg Effect, and Proliferation in the PTEN Pathway

Min Fang,[1] Zhirong Shen,[1] Song Huang,[1] Liping Zhao,[1] She Chen,[2] Tak W. Mak,[3] and Xiaodong Wang[1,2,*]
[1]Howard Hughes Medical Institute and Department of Biochemistry, University of Texas Southwestern Medical Center at Dallas, 5323 Harry Hines Boulevard, Dallas, TX 75390, USA
[2]National Institute of Biological Sciences, Zhongguancun Life Science Park, Beijing 102206, China
[3]The Campbell Family Institute for Breast Cancer Research, Princess Margaret Hospital, Toronto, ON M5G 2M9, Canada
*Correspondence: xiaodong.wang@utsouthwestern.edu
DOI 10.1016/j.cell.2010.10.010

SUMMARY

PI3K and PTEN lipid phosphatase control the level of cellular phosphatidylinositol (3,4,5)-trisphosphate, an activator of AKT kinases that promotes cell growth and survival. Mutations activating AKT are commonly observed in human cancers. We report here that ENTPD5, an endoplasmic reticulum (ER) enzyme, is upregulated in cell lines and primary human tumor samples with active AKT. ENTPD5 hydrolyzes UDP to UMP to promote protein N-glycosylation and folding in ER. Knockdown of ENTPD5 in PTEN null cells causes ER stress and loss of growth factor receptors. ENTPD5, together with cytidine monophosphate kinase-1 and adenylate kinase-1, constitute an ATP hydrolysis cycle that converts ATP to AMP, resulting in a compensatory increase in aerobic glycolysis known as the Warburg effect. The growth of PTEN null cells is inhibited both in vitro and in mouse xenograft tumor models. ENTPD5 is therefore an integral part of the PI3K/PTEN regulatory loop and a potential target for anticancer therapy.

INTRODUCTION

Class I phosphatidylinositol 3-kinases (PI3Ks) and lipid phosphatase PTEN balance cellular response to growth and survival signals (reviewed by Engelman et al., 2006). In response to activation of receptor tyrosine kinases, PI3K phosphorylates phosphatidylinositol 4,5-bisphosphate (PIP2) at the 3-OH position of the inositol ring to generate phosphatidylinositol 3,4,5-trisphosphate (PIP3) that recruits and activates serine/threonine kinase AKT (Whitman et al., 1988; Franke et al., 1997; Stephens et al., 1998). AKT subsequently activates many downstream targets for cell growth and survival, including the rapamycin-sensitive mTOR complex 1 (mTORC1), which then phosphorylates p70S6K and translation initiation factor 4E-BP1 to accelerate the translational rate, thus accommodating rapid growth (Fingar et al., 2002). PTEN, by dephosphorylating PIP3 back to PIP2, antagonizes the signal generated by PI3K (Maehama and Dixon, 1998). The importance of the PI3K/PTEN pathway has been manifested by frequent PI3K gain of function, or PTEN loss of function, in a variety of human cancers (reviewed by Yuan and Cantley, 2008; Keniry and Parsons, 2008).

AKT activation also contributes to the elevation of aerobic glycolysis seen in tumor cells, known as the Warburg effect (Elstrom et al., 2004; Warburg, 1925). AKT promotes cell-surface expression of glucose transporters while sustaining activation of hexokinase and phosphofructose kinase-1 (PFK1), thus accelerating influx and capture of glucose for glycolysis (reviewed by Vander Heiden et al., 2009). Of interest, in cancer cells, there is invariant expression of the embryonic M2 splice version of pyruvate kinase, an enzyme working in the last step of glycolysis, instead of a more active M1 splicing isoform expressed in most of the adult tissues (Christofk et al., 2008). The combined effects of more glucose entering into the glycolysis pathway and slowing down pyruvate kinase activity build up intermediate metabolites for synthesis of growth-enabling macromolecules. One noticeable example is the entry of glucose-6-phosphate to the pentose shunt pathway to generate ribose for nucleotide synthesis (reviewed by Vander Heiden et al., 2009).

Another outlet of glucose-6-phosphate is to form UDP-glucose, a substrate for protein glycosylation. In mammalian cells, most secreted proteins and membrane proteins are glycosylated at the asparagine (Asn) sites, i.e., N-glycosylated. Of interest, receptor tyrosine kinases that promote cell growth and proliferation, such as the epidermal growth factor receptor, EGFR, are much more highly N-glycosylated than receptors whose functions do not (Lau et al., 2007). Most of the glycosylation reactions happen in the Golgi apparatus, with two known exceptions. One is the dolichol-linked 14 sugar core glycan ($Glc_3Man_9GlcNAc_2$) that is synthesized in cytoplasm and ER membrane before being flipped into the lumen of ER, where it is transferred to the Asn of the nascent polypeptide chain (reviewed by Helenius and Aebi, 2004). Another is reglucosylation in ER after the third and second glucose (Glc) on the core glycan are trimmed by glycosidase I and II. Trimming and reglucosylation by UDP-glucose:glycoprotein glucosyltransferase (UGGT) generate monoglucosylated structures that are recognized by

calnexin/calreticulin, an ER molecular chaperone system for N-glycosylated proteins (reviewed by Ellgaard et al., 1999). The removal and addition of glucose allow the binding and release of calnexin/calreticulin to and from nascent polypeptide chains until the proteins are correctly folded and transferred to Golgi for further glycosylation. If proteins are misfolded beyond repair, they are subjected to degradation by the ER-associated protein degradation system (ERAD) (reviewed by Fewell et al., 2001).

During a study using the embryonic fibroblasts (MEFs) from the PTEN null mice and PTEN heterozygous littermates (Stambolic et al., 1998), we made a surprising finding that an ER UDP hydrolysis enzyme is upregulated by AKT activation. This enzyme, ENTPD5, seems to mediate many of the observed cancer-related phenotypes associated with AKT activation.

RESULTS

PTEN Knockout MEFs Have an Elevated Activity that Hydrolyzes ATP to AMP

As reported previously, the PTEN null MEFs showed elevated levels of phosphorylated AKT and p70S6 kinase, whereas the total protein level of these two kinases remained the same as in PTEN heterozygous MEFs (Stambolic et al., 1998) (Figure 1A). We noticed that S-100 cell extracts (prepared after collecting the supernatants of 100,000 × g spin of broken cells) from PTEN null MEFs had a lower ATP level compared to that from the heterozygous MEFs (Figure 1B, columns 7 and 8). Given that cellular ATP levels are relatively stable, we reasoned that the difference in their ATP contents occurred during S-100 preparation, which took about 1 hr. Indeed, as shown in Figure 1B, the ATP levels in PTEN null MEFs were only slightly lower than those in the heterozygous MEFs if the measurement was carried out immediately after cells were harvested (Figure 1B, columns 1 and 2). When the broken cell suspension, or supernatants after 10,000 × *g* spin (S-10), or S-100 were incubated on ice for 1 hr before the ATP levels were measured, ATP concentrations in the extracts from PTEN knockout MEFs were much lower than those from heterozygous MEFs (Figure 1B, columns 3–8). Such an observation indicated that there was higher ATP hydrolysis activity in the PTEN knockout cell extracts. To measure this activity directly, we incubated α-P^{32}-ATP with the S-100 extracts and analyzed the radioactivity using thin layer chromatography. As shown in Figure 1C, more radiolabeled ATP was hydrolyzed when incubated with the S-100 from PTEN null MEFs, and the nucleotide was hydrolyzed all the way to AMP.

To sort out whether the accelerated ATP hydrolysis was due to a specific activity or a combination of nonspecific ATPases, we fractioned the same amount of S-100 extracts from PTEN null and PTEN heterozygous MEFs side by side on a Q Sepharose ion-exchange column. The fractions from each column run were dialyzed, and ATPase activity was measured by adding each column fraction to the S-100 from PTEN heterozygous MEF, which served as the baseline activity. A single peak of elevated ATP-to-AMP activity centered at fractions 11–13 was observed in fractionated S-100 from PTEN null MEFs, whereas much less activity was seen in the corresponding fractions from PTEN heterozygous MEFs (Figure 1D).

ENTPD5 Is Responsible for the Elevated ATPase Activity in PTEN Knockout Cells

We decided to purify the ATPase from large-scale cultured PTEN knockout MEFs. We took 800 mg of S-100 from PTEN null MEFs and put it through five chromatographic steps (Figure 2A). The ATP hydrolysis activity was measured as in Figure 1D, and the active fractions from each column step were pooled, dialyzed, and loaded onto the next column. Finally, after a Superdex 200 gel-filtration column, the active fractions were loaded onto a 100 μl Mini Q column and the bound protein was eluted with a linear salt gradient. Fractions of 100 μl were collected and assayed. Shown in Figure 2B, a single ATP hydrolysis peak centered at fraction 6 was observed. When these fractions were analyzed by SDS-PAGE followed by silver staining, a protein band just below the 50 kDa molecular weight marker correlated perfectly with the activity.

This protein was excised from the gel and subjected to mass spectrometry analysis. The enzyme was identified as *ecto*nucleoside *triphos*phate *di*phosphohydrolase 5, ENTPD5, a member of the ENTPD enzyme family known to hydrolyze tri- and/or diphospshonucleotide to monophosphonucleotide (reviewed by Robson et al., 2006).

To verify that ENTPD5 is indeed the enzyme that caused the higher rate of ATP-to-AMP conversion in PTEN null MEFs, we first did a western blotting analysis of ENTPD5 in these MEFs. As shown in Figure 2C (bottom), ENTPD5 was only prominently detected in PTEN null extracts, but not in PTEN heterozygous extracts (Figure 2C, lanes 1 and 2). When mouse ENTPD5 was exogenously expressed in the PTEN heterozygous MEFs, the extracts from these cells showed the ability to hydrolyze ATP to AMP just like that from PTEN null cells (Figure 2C, lanes 3–5). Moreover, when ENTPD5 was knocked down in PTEN null MEFs with two different siRNA oligos, the ATP-to-AMP conversion was diminished in each case, and a control siRNA oligo had no effect (Figure 2C, lanes 6–10).

To confirm that the elevated level of ENTPD5 is due to deletion of PTEN, we transfected a wild-type PTEN cDNA, or the phosphatase active site mutant (PTEN C124S), into PTEN null MEFs. Indeed, restoring PTEN expression in these cells lowered phosphoAKT and diminished ENTPD5 expression, whereas the catalytically dead mutant PTEN had no effect (Figure 2D, lanes 2 and 3). Consistently, treatment of PTEN null MEFs with a PI3 kinase inhibitor also lowered the level of ENTPD5 (Figure 2E, lanes 2 and 3).

The upregulation of ENTPD5 in PTEN null cells is at transcriptional level. Its mRNA is 6-fold higher in PTEN null MEFs compared to that in PTEN heterozygous MEFs (Figure S1 available online). The promoter region of ENTPD5 is negatively regulated by the FoxO family of transcription factors (Figure S2), which upon phosphorylation by AKT, are displaced from the nucleus into the cytoplasm (Brunet et al., 1999).

To directly demonstrate the nucleotide hydrolysis activity of ENTPD5, we generated recombinant human ENTPD5 protein in insect cells using a baculovirus vector and purified the enzyme to homogeneity (Figure 3A, right). The purified enzyme was then incubated with ATP, ADP, CTP, CDP, GTP, GDP, UTP, and UDP, and the released phosphate was measured. Unexpectedly, the purified recombinant ENTPD5 could only hydrolyze UDP and GDP (Figure 3A, left).

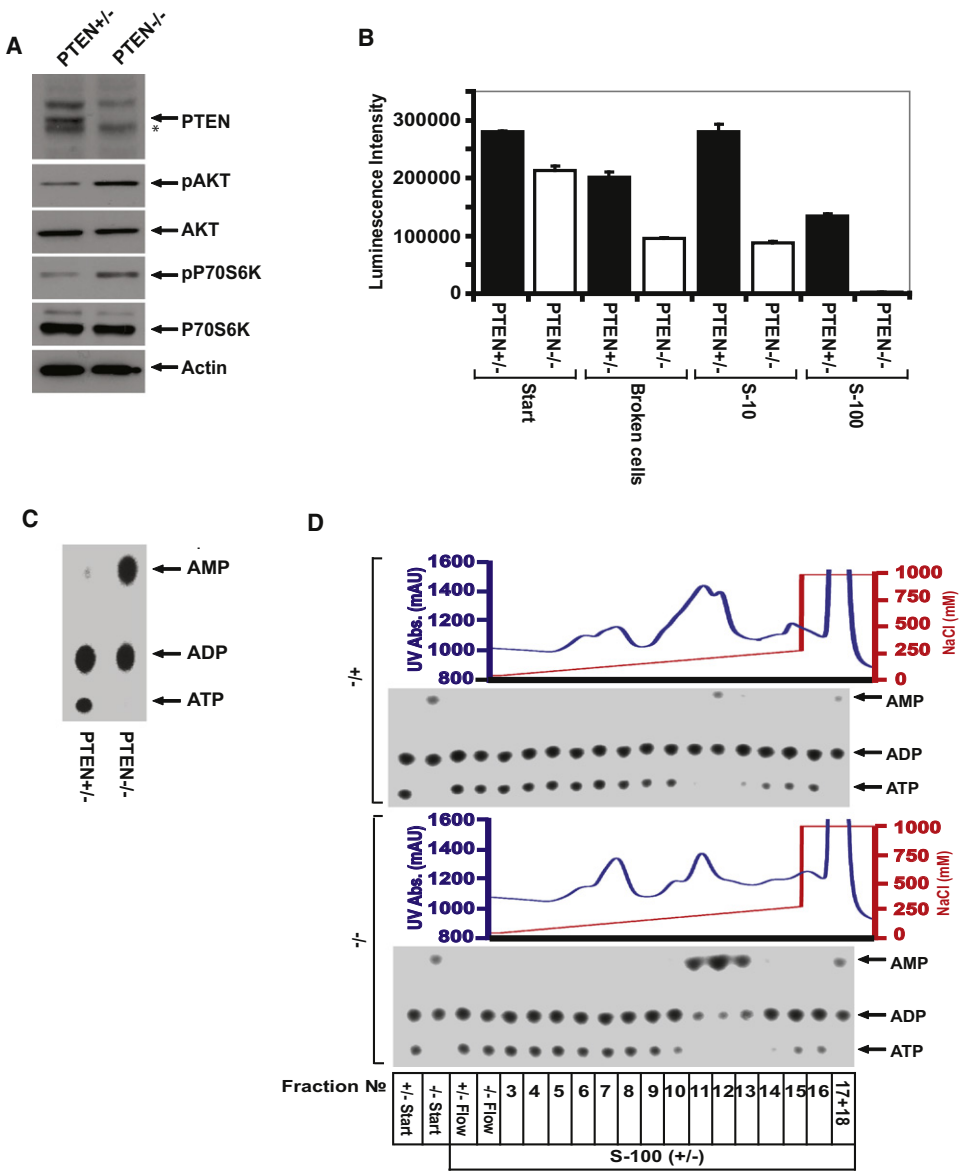

Figure 1. Identification of ATP Hydrolysis Activity in PTEN Knockout MEF Cells

(A) Total cell extracts from *PTEN*$^{+/-}$ and *PTEN*$^{-/-}$ cells were prepared as described in Experimental Procedures. Aliquots of 10 μg protein were subjected to 10% SDS-PAGE followed by western analysis of PTEN (asterisk denotes a cross-reactive band), phosphorylated AKT (pAKT), AKT, phosphorylated P70S6 kinase (pP70S6K), P70S6 kinase, and β-actin.

(B) Cell extracts were prepared from *PTEN*$^{+/-}$ and *PTEN*$^{-/-}$ cells, and at indicated steps of preparation, aliquots of 20 μl samples were incubated on ice for 1 hr followed by immediate measurement of ATP using a Cell Titer-Glo kit. Error bar represents standard deviation of two independent experiments.

(C) Aliquots of 30 μg of S-100 fractions from *PTEN*$^{+/-}$ or *PTEN*$^{-/-}$ cells were incubated with α-P^{32}-labeled ATP and analyzed by TLC as described in the Experimental Procedures. Positions for ATP, ADP, or AMP were indicated.

(D) 6 ml each of S-100 from *PTEN*$^{+/-}$ or *PTEN*$^{-/-}$ cells (3.5 mg/ml) was separated by a 1 ml Q Sepharose HP column with a salt gradient elution as indicated. Fractions of 1 ml were collected and dialyzed overnight at 4°C. 10.5 μl of each fraction was mixed with another 10.5 μl of undialyzed S-100 from *PTEN*$^{+/-}$ cells and assayed for ATP hydrolysis activity as in (C). The positions of ATP, ADP, and AMP were indicated. FPLC histograms were presented in top panels.

UMP or GMP Is a Required Cofactor for the ATP Hydrolysis Activity

During our ENTPD5 purification efforts, we noticed that a small molecule cofactor was required for the observed ATP-to-AMP hydrolysis activity. S-100 extracts from PTEN null MEFs lost ATP-to-AMP converting activity after dialysis (Figure 3B, lane 4), and the activity was restored with addition of a small molecule fraction prepared by a 10 kDa cutoff filter (Figure 3B, lane 6). There was no difference in such a small molecule in PTEN heterozygous and PTEN null MEFs (Figure 3B, lanes 6

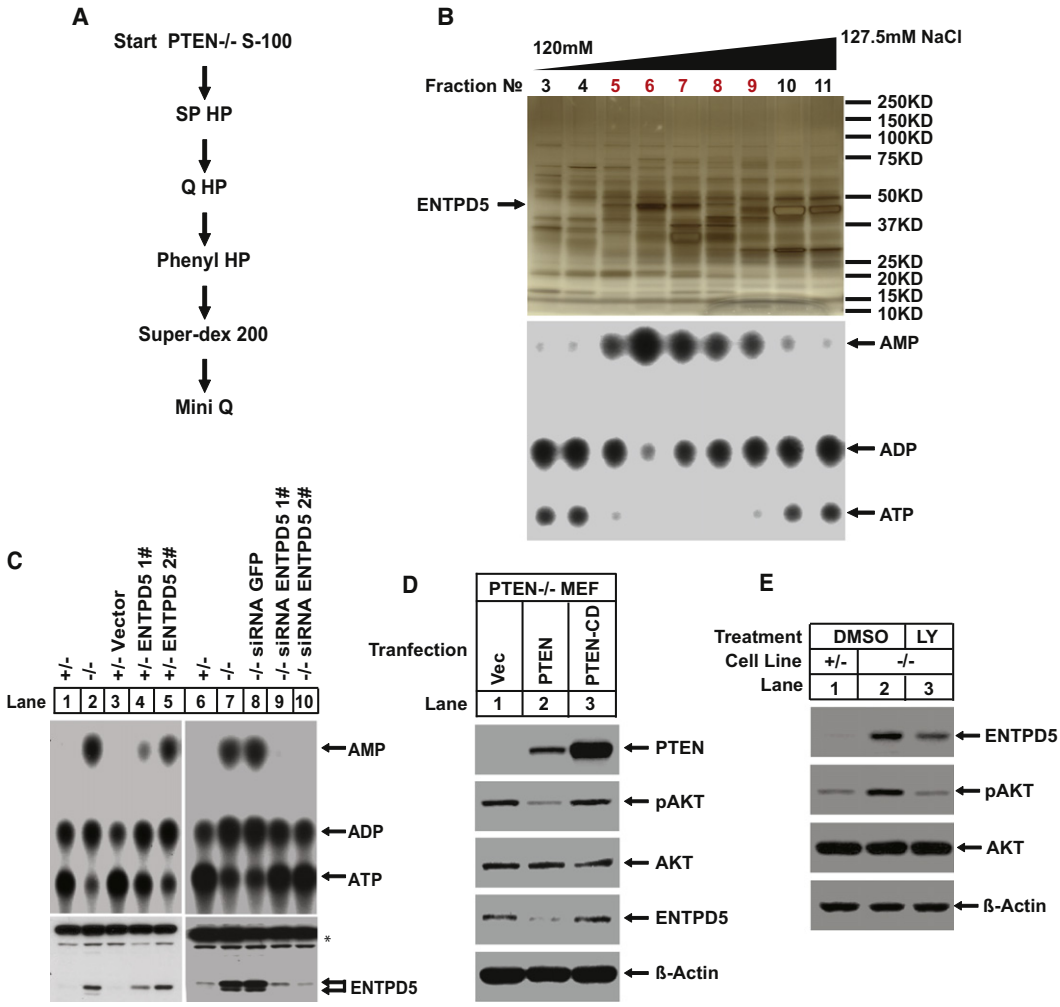

Figure 2. Purification and Characterization of ENTPD5

(A) Diagram of the purification scheme for ATP hydrolysis activity from S-100 of *PTEN*$^{-/-}$ MEF cells.

(B) Final step of purification. (Top) Aliquots of 30 μl of indicated fractions from the Mini Q column were subjected to 4%–10% gradient SDS-PAGE gels followed by staining using a silver staining kit from Invitrogen. (Bottom) Aliquots of 3 μl of indicated fractions were incubated with 10.5 μl of undialyzed S-100 from *PTEN*$^{+/-}$ MEF cells and assayed for ATP hydrolysis activity.

(C) (Lanes 1–5) ATP hydrolysis activity in S-100 from *PTEN*$^{+/-}$ MEF cells expressing exogenous ENTPD5. *PTEN*$^{+/-}$ vector or *PTEN*$^{+/-}$ ENTPD5 1# and 2# (two individual clones with different expression levels of ENTPD5) were established as described in the Experimental Procedures. Cell lysates (S-100) from indicated cell lines were prepared, and aliquots of 30 μg were used for ATP hydrolysis assay. (Lanes 6–10) ENTPD5 expression in *PTEN*$^{-/-}$ MEFs was knocked down as described in the Experimental Procedures. The cells were harvested, and S-100 were prepared and normalized for ATP hydrolysis assay. Positions of ATP, ADP, and AMP are indicated. (Bottom) Aliquots of 10 μg protein of indicated samples were subjected to 10% SDS-PAGE followed by western analysis of ENTPD5. Asterisk denotes cross-reactive proteins.

(D) *PTEN*$^{-/-}$ MEF cells were transfected with 4 μg plasmid DNA containing vector control or cDNA encoding PTEN or PTENcs as indicated. At 24 hr after transfection, cells were harvested and total cell lysates were prepared. Aliquots of 10 μg of protein were loaded onto 10% SDS-PAGE followed by western analysis of levels of PTEN, AKT, phosphorylated AKT(pAKT), ENTPD5, and β-actin as indicated.

(E) *PTEN*$^{+/-}$ and *PTEN*$^{-/-}$ MEF cells were treated with DMSO or LY294002 (50 μM) for 24 hr. Aliquots of 20 μg total cell extracts were subjected to 10% SDS-PAGE followed by western analysis using indicated antibodies.

See also Figure S1 and Figure S2.

and 8), and the molecule was also present in S-100 from HeLa cells (Figure 3B, lane 10), which have a wild-type PTEN.

Based on its biochemical properties, we deduced that the cofactor is a nucleotide. Testing a variety of nucleotides revealed that uracil and guanine, either in tri-, di-, or monophosphate form, substituted the small molecule fraction from cells (Figure 3C, lanes 1–15). In contrast, thymidine nucleotides have no activity, whereas CMP only showed a slight activity.

To see whether the conversion of UTP/UDP to UMP is necessary for the observed activity, we tested various forms of nonhydrolyzable uracil, including UTPγS, UTPαS, and UMP-PNP (Figure 3D). All of these nucleotides worked except UTPαS,

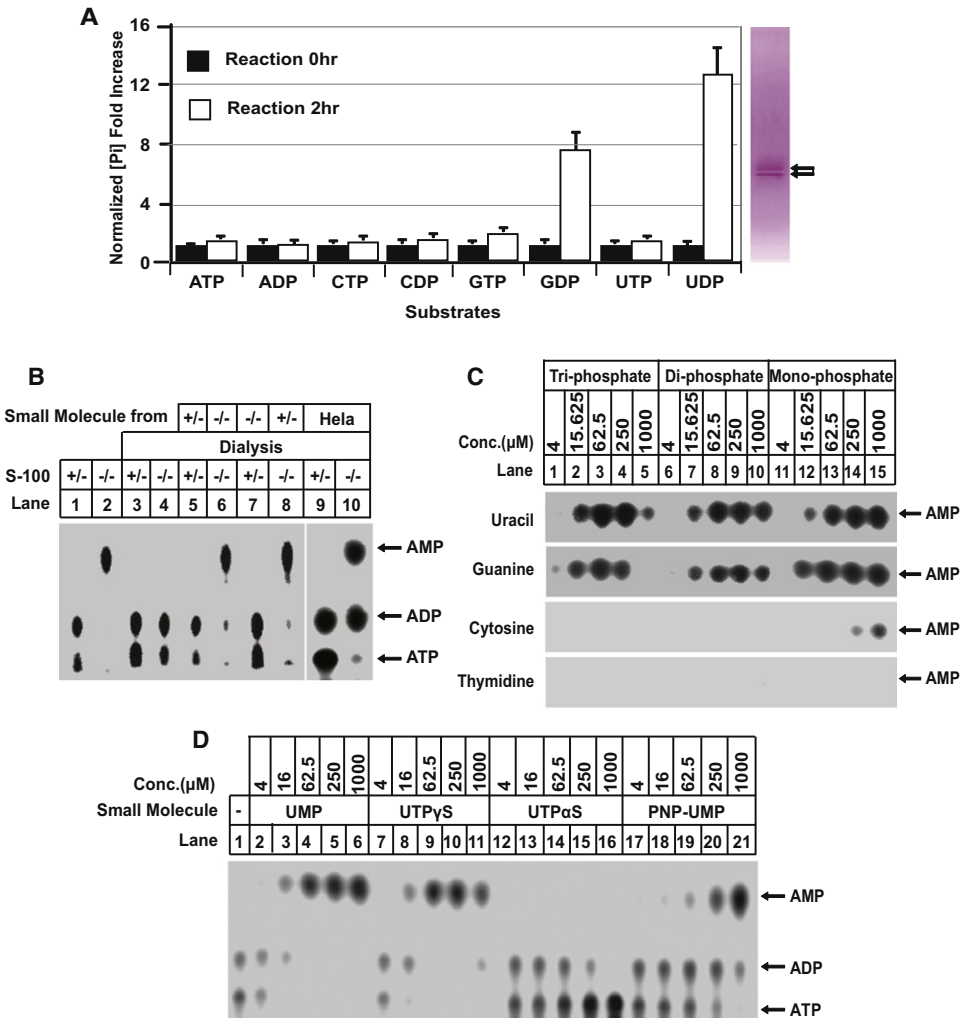

Figure 3. Small Molecule Requirement for ENTPD5-Mediated ATP Hydrolysis

(A) (Right) the recombinant human ENTPD5 was generated and purified as described in the Experimental Procedures. An aliquot of 120 ng recombinant ENTPD5 was subjected to SDS-PAGE followed by Coomassie brilliant blue staining. Arrows indicate recombinant ENTPD5. (Left) The nucleotide hydrolysis reactions were carried out in triplicate by mixing 0.1 mg/ml ENTPD5 with 50 μM indicated nucleotides. After 2 hr incubation at 30°C, released free phosphate was measured by malachite green assay as described in the Experimental Procedures. Data shown are representative of three independent experiments. Error bars indicate SEM.

(B) Small molecule (<10 kDa) was extracted from either *PTEN*$^{+/-}$ or *PTEN*$^{-/-}$ MEF cells or HeLa S3 cell lysates (S-100 fractions) as described in the Experimental Procedures. Aliquots of 10.5 μl undialyzed cell lysates (lane 1 and 2) or dialyzed cell lysates (lane 3–10) from *PTEN*$^{+/-}$ (lanes 1, 3, 5, 7, and 9) or *PTEN*$^{-/-}$ (lanes 2, 4, 6, 8, 10) MEFs (3.5 mg/ml) were mixed with another 10.5 μl buffer A (lane 1 to 4) or small molecule recovered from *PTEN*$^{+/-}$ (lanes 5 and 8), *PTEN*$^{-/-}$ cells (lanes 6 and 7), or from HeLa S3 cells (lanes 9 and 10) and were assayed for ATP hydrolysis activity. The positions of ATP, ADP, and AMP were indicated.

(C) Aliquots of 10.5 μl dialyzed S-100 from *PTEN*$^{-/-}$ MEF cells (3.5 mg/ml) were incubated in the presence of indicated final concentration of UTP, UDP, and UMP; or GTP, GDP, and GMP; or CTP, CDP, and CMP; or TTP, TDP, and TMP as indicated at 30°C with α-P^{32}-labeled ATP in a total volume of 30 μl at 30°C for 1 hr followed by TLC to resolve radioactive adenosine nucleotides. Position of AMP on TLC plate is indicated.

(D) Aliquots of dialyzed S-100 prepared from *PTEN*$^{-/-}$ MEF cells were mixed with buffer A (lane 1) or indicated final concentration of indicated nucleotides and assayed for ATP hydrolysis activity.

See also Figure S3.

which could not be hydrolyzed to UMP, indicating that the conversion to UMP is critical for this cofactor to function. The same holds true for guanine nucleotides (Figure S3).

UMP, ENTPD5, UMP/CMP Kinase-1, and Adenylate Kinase-1 Constitute an ATP-to-AMP Hydrolysis Cycle

Based on the facts that purified ENTPD5 is unable to hydrolyze ATP directly and the assay also contained S-100 from PTEN heterozygous MEFs, we realized that there must be more factors in the S-100, which are also required to hydrolyze ATP to AMP. These factors presented in cells regardless of their PTEN status. For example, when we added purified, recombinant ENTPD5 and UMP to the dialyzed S-100 from large-scale cultured HeLa cells, the ATP-to-AMP hydrolysis was reconstituted (Figure 4A, lanes 1–6). This observation made purification of these factors easier because HeLa cells can be grown in large quantity in

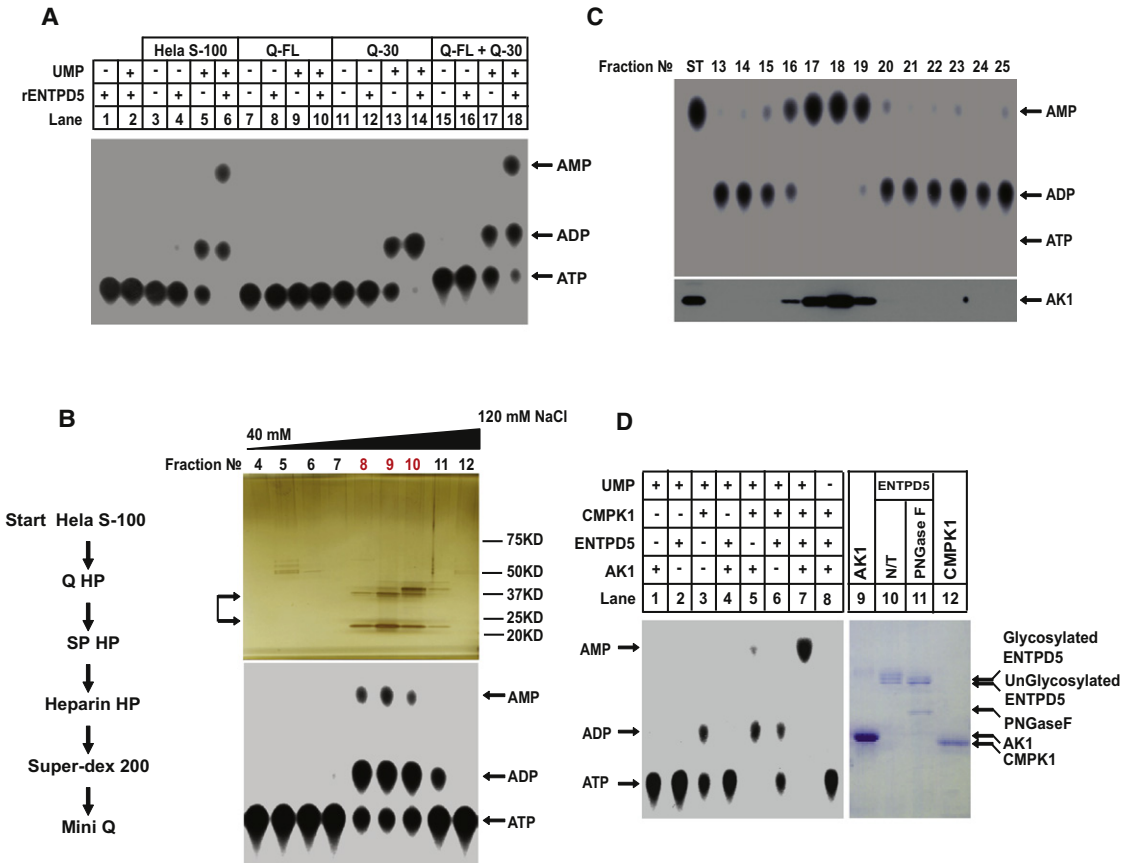

Figure 4. Reconstitution of ENTPD5-Mediated ATP Hydrolysis

(A) HeLa S3 cell S-100 was fractionated by Q Sepharose column to two fractions (Q-FL [flowthrough] and Q-30). Q-30 represents fraction eluted with 300 mM NaCl. Aliquots of 15 μl buffer A (lane 1 and 2), or dialyzed HeLa cell S-100 (lanes 3–6), or Q-FL (lanes 7–10), or Q-30 (lanes 11–14), or Q-FL combined with Q-30 (7.5 μl each) (lanes 15–18) were mixed with (lanes 1, 2, 4, 6, 8, 10, 12, 14, 16, and 18) or without (lanes 3, 5, 7, 9, 11, 13, 15, and 17) ENTPD5 in the presence (lanes 2, 5, 6, 9, 10, 13, 14, 17, and 18) or absence (lanes 1, 3, 4, 7, 8, 11, 12, 15, and 16) of 100 μM UMP and assayed for ATP hydrolysis activity.

(B) (Left) Diagram of the purification scheme for the required factor in Q-30. (Right) Final step of purification of CMPK1. (Top) Aliquots of 60 μl indicated Mini Q fractions that were subjected to 4%–10% gradient SDS-PAGE followed by silver staining. Arrow indicates the protein band correlated with ATP hydrolysis activity. (Bottom) Aliquots of 5 μl indicated fractions that were mixed with 15 μl of dialyzed Q-FL fraction in the presence of 100 μM UMP and 18 ng recombinant ENTPD5 and were assayed for ATP hydrolysis activity.

(C) 3 ml of the Q-FL fraction was concentrated to 600 μl with a spin column and analyzed on a Supdex-200 column (10/30). Fractions of 1 ml were collected, and aliquots of 7.5 μl of indicated fractions were combined with 7.5 μl dialyzed Q-30 fraction, 100 μM UMP, and 18 ng recombinant ENTPD5 and were assayed for ATP hydrolysis activity. Positions of radioactive ATP, ADP, and AMP are indicated. (Bottom) Aliquots of 10 μl of indicated fractions were subjected to 10% SDS-PAGE followed by western blotting analysis using an antibody against human adenylate kinase 1 (AK1).

(D) (Left) Aliquots of recombinant AK1 (lane 1), ENTPD5 (lane 2), and CMPK1 (lane 3) (final concentration, 1 μg/ml) were incubated alone or were sequentially combined as indicated (lane 4 to 8) in the presence (lane 1 to 7) or absence (lane 8) of UMP (100 μM) for ATP hydrolysis activity. Position of ATP, ADP, or AMP was indicated. (Right) Aliquots of 10 μg recombinant AK1 (lane 9), ENTPD5 (lane 10) or ENTPD5 pretreat with PNGase F (NEB) (50 units/μg ENTPD5) (lane 11), and CMPK1 (lane 12) were subjected to 10% SDS-PAGE followed by Coomassie brilliant blue staining.

suspension. To identify these factors, we fractionated HeLa cell S-100, using a Q Sepharose column, and collected both the flowthrough (Q-FL) and column-bound fractions eluted with 300 mM NaCl (Q-30). Neither fraction alone was able to hydrolyze ATP to AMP, although the Q-30 fraction, when ENTPD5 and UMP were present, hydrolyzed ATP to ADP (Figure 4A, lanes 13 and 14). When both the Q-FL and Q-30 fractions were included, the ATP-to-AMP activity was fully reconstituted (Figure 4A, lane 18).

We purified the activity present in the Q-30 fraction. The activity present in the Q-30 fraction was purified by subjecting HeLa S-100 onto four sequential column chromatographic steps and finally onto a Mini Q column (Figure 4B, left). The activity was eluted from this column with a linear salt gradient from 40 to 120 mM NaCl, and fractions eluted from the column were assayed in the presence of recombinant ENTPD5, UMP, and the Q-FL fraction (Figure 4B, right-bottom). A peak of activity was observed at fractions 8–10. The same fractions were subjected to SDS-PAGE followed by silver staining, and two protein bands close to 37 and 20 kDa markers correlated perfectly with activity (Figure 4B, right-top). Both bands were identified by mass spectrometry as human UMP/CMP kinase-1 (CMPK1).

The identification of UMP/CMP kinase in the Q-30 fraction shed light on why UMP is a cofactor for the ATPase activity and how ENTPD5 plus this enzyme generates ADP from ATP. In this reaction, UMP is phosphorylated into UDP by CMPK1 and ATP, generating ADP. UDP is subsequently hydrolyzed by ENTPD5 to UMP, completing the cycle with net conversion of ATP to ADP.

With this knowledge, we then made an educated guess that the third protein factor present in the Q flowthrough fraction should be an adenylate kinase, which converts two ADP into one ATP and AMP, causing the ATP-to-AMP conversion seen in PTEN null cell extracts. To confirm this, we took the Q flowthrough fraction and subjected it to a gel-filtration column and collected the fractions eluted from the column to assay for ATP-to-AMP hydrolysis in the presence of UMP, purified recombinant ENTPD5, and the Q-30 fraction that contains CMPK1. An ATP-to-AMP activity peak centered at fractions 17 and 18 was observed (Figure 4C, top). When these factions were subjected to western blotting analysis using an antibody against adenylate kinase-1 (AK1), the detected western blotting band correlated perfectly with the activity peak (Figure 4C, bottom). The correlation was maintained with additional chromatographic steps (data not shown).

We subsequently generated recombinant CMPK1 and AK1 in bacteria and purified them to homogeneity (Figure 4D, lanes 9 and 12). Purified recombinant ENTPD5 expressed in insect cells runs as a triplet on an SDS-PAGE gel that could be shifted down to a doublet after treatment by PNGase F, indicating that ENTPD-5 is glycosylated (Figure 4D, lanes 10 and 11).

These purified recombinant proteins allowed us to reconstitute the ATP-to-AMP hydrolysis cycle. Only when all three enzymes and UMP were present, efficient ATP-to-AMP conversion was observed (Figure 4D, lanes 1–8).

ENTPD5 Is an ER Enzyme

After purification and identification of ENTPD5 from PTEN null cells, we realized that ENTPD5 is identical to a previously purified ER UDPase (Trombetta and Helenius, 1999). Although we identified and purified ENTPD5 from the S-100, the enzyme most likely fractionated there as a result of broken ER from physical shearing during the cell-breaking process. When we expressed an ENTPD5-GFP fusion protein in cells, the GFP signal was colocalized with the coexpressed ER-DsRed marker (Figure 5A). The ER location of ENTPD5 and its preferred specificity for UDP suggested that ENTPD5 functions in the process of reglucosylation catalyzed by UGGT for calnexin/calreticulin-mediated protein folding (Trombetta and Parodi, 2003). In the process, UDP is generated after the conjugated glucose gets transferred to the glycosidase I/II trimmed core glycan on N-glycosylated proteins. UDP-glucose is made in cytosol and transported into ER through the UDP-sugar transporter, which is an antiporter that must exchange out one molecule of UMP for each UDP sugar conjugate imported into the ER (Hirschberg et al., 1998). UDP therefore needs to be hydrolyzed to UMP to prevent end product feedback inhibition of UGGT, as well as to serve as a substrate for the antiporter (Trombetta and Helenius, 1999). UMP is phosphorylated back to UDP by CMPK1 in the cytosol, and the generated ADP is converted to ATP and AMP by AK1 (diagramed in Figure 5B).

Knockdown of ENTPD5 Causes ER Stress and Growth Inhibition

Because cells with an activated PI3K/AKT pathway increase their cellular protein translation level, cells need to evolve a corresponding system in ER to accommodate the high demand for protein folding process. It is possible that cells may do so by upregulating ENTPD5 to increase the conversion of UDP to UMP in ER, thereby promoting N-glycosylation and folding. Thus, reducing the level of ENTPD5 in cells with active AKT should induce ER stress. In addition, because many growth-promoting cell membrane receptors are highly N-glycosylated, loss of function of ENTPD5 could affect their folding process, resulting in their reduction and, subsequently, cell growth arrest. To test this hypothesis, we engineered several cell lines based on the PTEN null MEFs in which the expression of ENTPD5 could be knocked down with the addition of doxcycline (Dox), which turned on a Tet-suppressor-controlled shRNA-targeting ENTPD5. The results from a representative cell line were shown in Figure 5C. Comparing to PTEN null MEFs expressing GFP shRNA, addition of Dox to the culture media resulted in successful knockdown of ENTPD5 expression in these cells. As a result, an ER stress marker, GRP78/BiP, was induced, and cellular N-glycosylation level, as measured by PHA blotting, was down (Figure 5C, lanes 5–8). Of interest, the levels of receptor tyrosine kinases, including EGFR, Her-2/Erb-2, and type I insulin-like growth factor receptor (IGF-IR) β, were significantly decreased after ENTPD5 knockdown.

To confirm that the above-mentioned cellular effects after ENTPD5-targeting shRNA expression were specific, we introduced into these cells a cDNA encoding ENTPD5 with silent mutations in the shRNA target sequence. In these cells, although the endogenous ENTPD5 was still knocked down after addition of Dox (Figure 5D, lanes 2, 4, and 6), the expression of an shRNA-resistant wild-type transgene (three flag tags were fused to ENTPD5 coding sequence so it migrated higher) led to complete reversal of BiP induction, lowered glycosylation, and downregulation of these growth factor receptors (Figure 5D, lane 4). In contrast, introducing an E171A mutant that abolishes UDP hydrolysis activity of ENTPD5 was not able to rescue these phenotypes (Figure 5D, lane 6). In addition to BiP, another ER stress marker, CHOP, was also induced when ENTPD5 was knocked down (Figure 5D).

Consistent with the loss of growth factor receptors after ENTPD5 knockdown, cell growth was also dramatically attenuated. As shown in Figure 5E, when ENTPD5 in PTEN null MEFs was knocked down after addition of Dox, very few colonies grew on the culture dish after 10 days, although the same number of cells was plated initially, and they were cultured under the same condition (Figure 5E, left row). The growth inhibition was rescued when the shRNA-resistant ENTPD5 cDNA was expressed (Figure 5E, middle row), whereas the inhibition was exacerbated if an enzymatic dead mutant of ENTPD5 was expressed instead (Figure 5E, right row).

ENTPD5 Promotes Aerobic Glycolysis

One implication of elevated ENTPD5 expression is that a significant percentage of cellular ATP is consumed through the ENTPD5/CMPK1/AK1 enzyme cascade. To maintain the

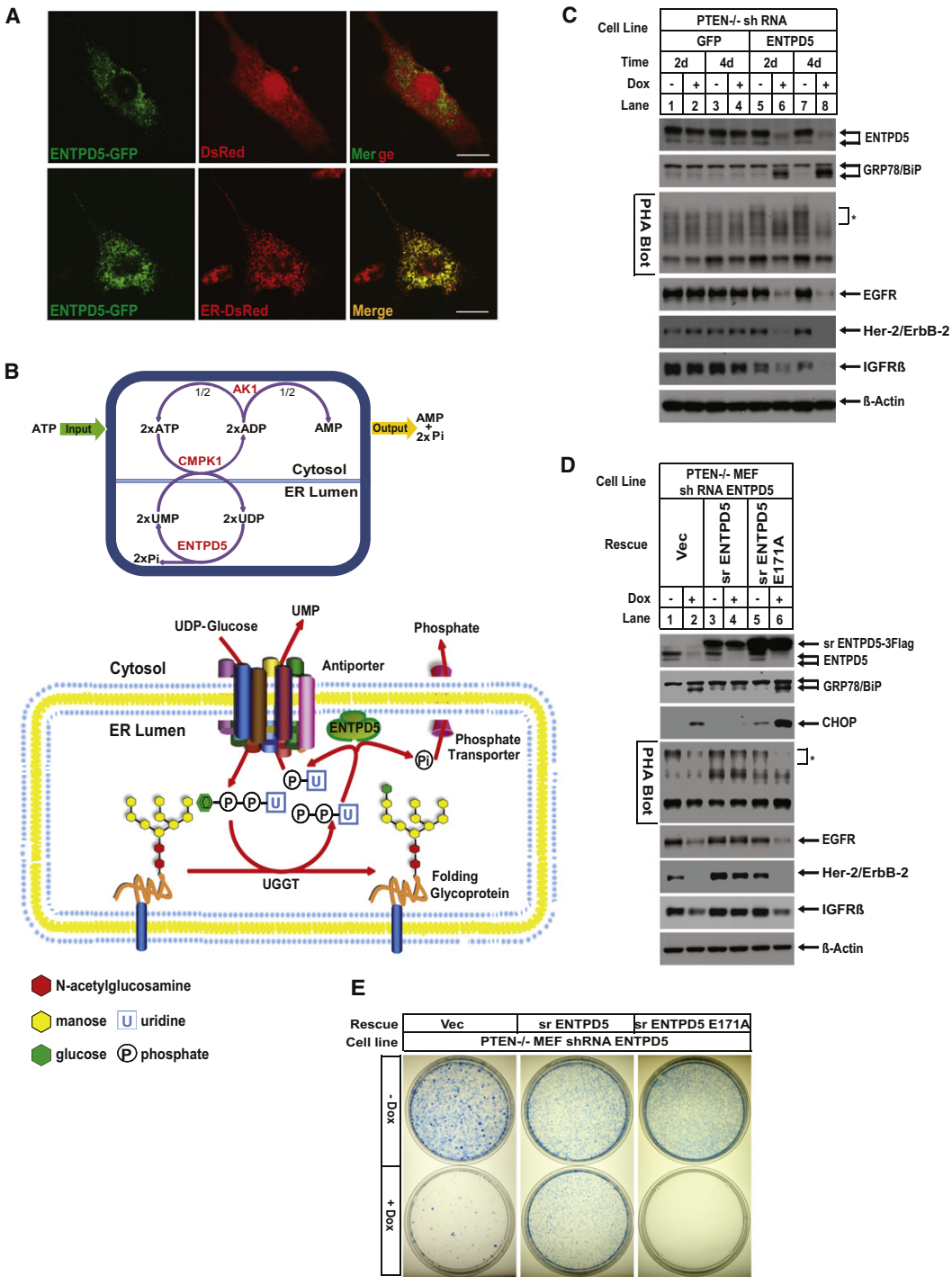

Figure 5. Biological Function of ENTPD5 in *PTEN*$^{-/-}$ MEF Cells

(A) *PTEN*$^{-/-}$ MEF cells were cotransfected with mouse ENTPD5-GFP and free DsRed or with ENTPD5-GFP and ER-localized DsRed (ER-DsRed). ENTPD5-GFP colocalized with ER-DsRed (bottom row), but no obvious codistribution with free DsRed was observed (top row). Scale bars, 10 μm.

(B) Working model for ENTPD5. See the text for details.

(C) *PTEN*$^{-/-}$ MEF cells with doxycycline (Dox)-inducible expression of shRNA-targeting ENTPD5 was generated as described in the Experimental Procedures. After 2 or 4 days induction with Dox (0.125 μg/ml), cells were harvested and total cell lysates were prepared as described in the Extended Experimental Procedures. Aliquots of 10 μg protein were subjected to SDS-PAGE followed by western blotting analysis using the indicated antibodies. Glycosylation was visualized by PHA blot as indicated. Asterisk denotes decreased glycosylated proteins.

intracellular ATP level, the extra ATP consumed should come from either increased oxidative phosphorylation or glycolysis. We therefore tested both by measuring oxygen consumption and lactate production, respectively. Consistent with previous reports, there was not much difference in the respiration rate of PTEN null and PTEN heterozygous MEFs (Figure S4), but PTEN null cells showed ~40% higher lactate production in their cultured medium (Figure 6A, columns 4 and 5). When ENTPD5 was ectopically expressed in two PTEN heterozygous MEF lines, lactate production was increased, and the level of increase correlated with that of ENTPD5 expression (Figure 6A, columns 2 and 3). Consistently, when ENTPD5 was knocked down with addition of Dox as in Figure 5D, lactate production was significantly decreased (Figure 6B, columns 1 and 2). In PTEN null MEFs harboring Dox-inducible ENTPD5-targeting shRNA that also expressed shRNA-resistant ENTPD5 transgene, addition of Dox did not result in a decrease in lactate production, and the basal lactate production also became higher, correlated with the higher than endogenous expression of the transgene (Figure 6B, columns 3 and 4, and Figure 5D). In contrast, when the catalytic site mutant ENTPD5 transgene was expressed to the similar level, lactate production still reduced with the addition of Dox (Figure 6B, columns 5 and 6).

If the ATP hydrolysis cycle initiated by ENTPD5 discovered in vitro is operational in cells, and the extra ATP consumed by a higher level of ENTPD5 is compensated by increased glycolysis, glucose starvation of these cells should result in much faster decrease of intracellular ATP level compared to cells with lower ENTPD5 expression. Indeed, when intracellular ATP concentrations in PTEN heterozygous and PTEN null MEFs were measured after glucose withdrawal from the culture media, that in PTEN null MEFs decreased to about half of the original level within the first hour, while there was little change of ATP in PTEN-heterozygous MEF within 2 hr (Figure 6C).

To confirm that the faster ATP level dropping in PTEN null cells was due to higher expression of ENTPD5, the same set of MEFs as in Figure 6B was subjected to glucose starvation after ENTPD5 was knocked down with the addition of Dox. Knockdown of ENTPD5 for 2 days in PTEN null MEFS caused the total cellular ATP level to decrease (Figure 6D, columns 3 and 4). However, the ATP level did not decrease further after glucose starvation for 1 hr, whereas cells without Dox treatment consumed 50% of original ATP during this period (Figure 6D, columns 1 and 2). The MEFs expressing the shRNA-resistant ENTPD5 did not lower their ATP level with Dox treatment, but their ATP levels were even more drastically lowered after glucose starvation, possibly due to ENTPD5 overexpression (Figure 6D, columns 5–8). In contrast, cells expressing a similar level of the catalytic dead mutant ENTPD5 behaved the same as cells without transgene expression (Figure 6D, columns 9–12).

The observed decrease of glycolysis after ENTPD5 knockdown could be due to lowered tyrosine kinases receptors and AKT activity (Figure 5C and Figure S5), which stimulates the glucose transporter activity on cell surface (Kohn et al., 1996; Plas et al., 2001). In addition, knockdown of ENTPD5 may reduce the production of ADP/AMP, which allosterically activate glycolysis enzymes such as phosphofructose kinase (PFK) (Gevers and Krebs, 1966). To distinguish these possibilities, cellular fructose-6-phosphate and fructose-1,6-bisphosphate were measured using LC-Mass. As shown in Figure 6E, the former was lowered by ~20% after ENTPD5 knockdown (Figure 6E, left), whereas the latter dropped by ~60% (Figure 6E, right). These results suggested that ENTPD5 indeed affects glucose influx to cells, but its major impact on glycolysis is to directly activate glycolysis enzymes such as PFK by hydrolyzing ATP.

ENTPD5 Expression Correlates with AKT Activation in Human Cancer Cell Lines and Primary Tumor Samples

PTEN mutation and AKT activation are common features for human cancer. To check whether what was observed in PTEN null MEFs is also true for human cancer cells, we screened a panel of human cancer cell lines for the expression of PTEN, activated AKT, and ENTPD5. As shown in Figure 7A, AKT activation was seen in human prostate cancer lines C42 and LNCaP cells, and in these two cell lines, elevated ENTPD5 expression was also observed.

We also examined ENTPD5 expression and AKT activation in primary human tumor samples by staining two adjacent sections from a formalin-fixed, paraffin-embedded human primary prostate cancer sample with rabbit monoclonal antibodies against human ENTPD5 and phosphoAKT, respectively. The specificity of this anti-ENTPD5 antibody was verified by western blotting analysis using LNCaP cell lines with or without their ENTPD5 knocked down (Figure S6A). The staining intensity for ENTPD5 in tumor was significantly greater compared with adjacent normal tissue and was correlated with pAKT staining (Figure 7B). Out of 10 samples from patients between age 57 and 76, only one tumor sample from a 57-year-old patient and another sample collected from a patient who had just gone through therapy did not show strong ENTPD5 staining, and the same tumors were also negative for pAKT (Figure S6B2 and Figure S6B10). The remaining eight samples all showed greater tumor staining of pAKT and ENTPD5 (Figure 7B and Figures S6B3–S6B9).

Because microarray data of many tumors are publicly available, we also analyzed a group of recently publicized microarray data from human prostate cancer samples (Bermudo et al., 2008). We found that ENTPD5 is highly expressed in all 20 tumor samples compared to normal prostate epithelium cells (Figure S7). In addition, after clustering all gene expression profiles from prostate tumor microarray data using SOM (self-organization method), we identified dozens of genes associated with AKT activation, including Her-3, PI3KCB, Ras, S6 kinase, CD36, IL8, EGF, osteropontin, and FoxO1, which are significantly coregulated with ENTPD5 (Figure S7).

(D) Rescue cell lines with expression of shRNA-resistant wild-type or catalytic dead mutant (E171A) ENTPD-5 were established as described in the Extended Experiments Procedures. Same as in (C), after 2 days culture, cells were harvested, and total cell lysates (10 μg/lane) were subjected to SDS-PAGE followed by western analysis as indicated. Glycosylation was visualized by PHA blot analysis.

(E) Rescue cell line was plated at density of 5×10^4/100 mm dish and treated with Dox as in (C). Cell medium was changed each 3 days. After 10 days culture, the plates were stained by methylene blue.

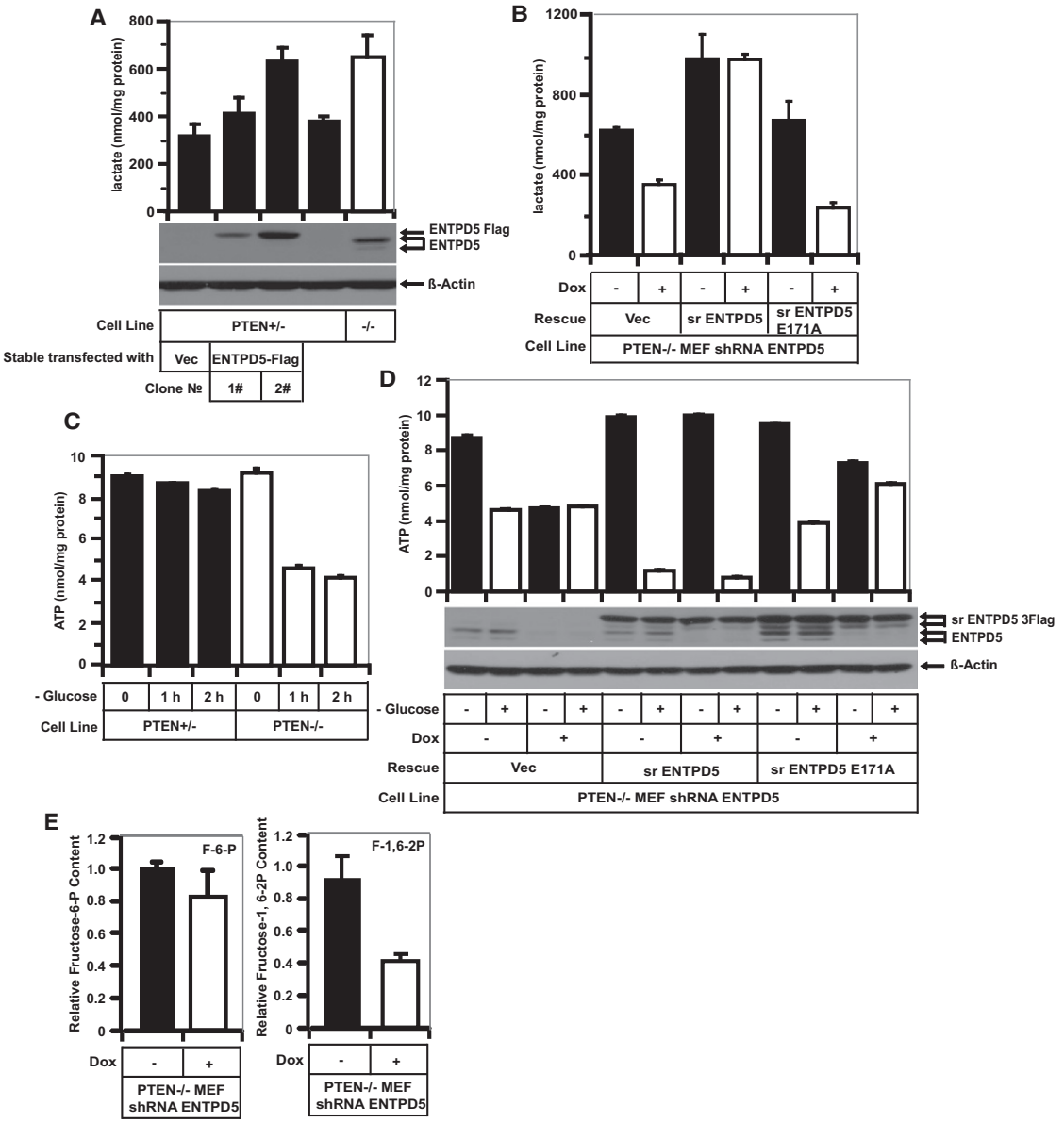

Figure 6. ENTPD5 Promotes ATP Hydrolysis and Glycolysis In Vivo

(A) Lactate in the culture media of *PTEN*$^{+/-}$ and *PTEN*$^{-/-}$ MEF cells (columns 4 and 5) as well as *PTEN*$^{+/-}$ MEF clones stably transfected with vector control (column 1) or Flag-tagged mouse ENTPD5 (column 2, clone 1 and column 3, clone 2, as used in Figure 2C) was measured as described in the Extended Experimental Procedures, and the value was normalized to total protein amount.

(B) Lactate in the culture media of ENTPD5 knockdown and rescue cell lines was measured as in (A) except pretreatment with or without Dox for 2 days.

(C) *PTEN*$^{+/-}$ and *PTEN*$^{-/-}$ MEF were deprived of glucose for indicated time periods, and intracellular ATP was determined as described in Extended Experimental procedures.

(D) The intracellular ATP was measured 1 hr after glucose starvation on ENTPD5 knockdown and rescue cell lines as in (B).

(E) ENTPD5 was knocked down as in (B), and the intracellular fructose-6-phosphate (left) and fructose-1,6-bisphosphate (right) were separated and quantified by HPLC mass spectrometry (ABI 3200 Q TRAP LC/MS/MS Systems). The relative amount of metabolite is normalized to total ion count (TIC). All experiments were repeated at least two times, and the error bar represents standard deviation.

See also Figure S4 and Figure S5.

ENTPD5 Is Important for Cancer Cell Growth

To verify the functional significance of ENTPD5 expression in human cancer cells, we generated a cell line from the original LNCaP cells in which an shRNA against human ENTPD5 could be induced by Dox. In these cells, knockdown of ENTPD5 by adding Dox to the culture media also lowered N-glycosylation (Figure 7C, comparing lanes 7 and 8, 9 and 10, and 11 and 12) and induced BiP expression (Figure 7C, lanes 8, 10, and 12).

These phenotypes were rescued by the expression of a wild-type shRNA-resistant ENTPD5 transgene, but not by the active site mutant ENTPD5 (Figure 7C, lanes 13–24). Several growth factor receptors were also checked in these cell lines after Dox treatment. As shown in Figure 7D, EGFR and Her2/ErbB-2 were significantly down, and IGFRβ was slightly down (Figure 7D, lanes 1–4). They were restored to the normal level by the expression of shRNA-resistant ENTPD5 transgene (Figure 7D, lanes 5 and 6), but not the active site mutant (Figure 7D, lanes 7 and 8). Consistently, when the cell number was measured after 4 day knockdown of ENTPD5, only about half of LNCaP cells were there, compared to a control knockdown cell line, and the defect was rescued by expression of wild-type ENTPD5 transgene, but not active site mutant (Figure 7E).

To test whether knocking down ENTPD5 in LNCaP cells also has an effect on their growth in vivo, we implanted the LNCaP cells bearing a Dox-inducible shRNA targeting ENTPD5 in matrigel in nude mice. As a control, LNCaP cells with a Dox-inducible shRNA targeting GFP were also implanted. After the xenograft tumors reached the size of 500 mm^3, a cohort of seven mice were fed with Dox-containing water. The level of ENTPD5 in these tumors was measured after 6 weeks. Compared with mice fed with normal water, the ENTPD5 levels in ENTPD5-targeting shRNA containing tumors from mice fed with Dox-containing water were significantly lower except in one mouse (Figure 7F). Whereas ENTPD5-targeting shRNA containing tumors in mice fed with normal water continued to grow, the tumors in mice fed with Dox-containing water shrank (Figure 7G). Amazingly, when these tumor samples were analyzed under a microscope after fixing and staining with hematoxylin and eosin, there were very few tumor cells left in the matrigel in tumors grown in Dox-fed mice, whereas in mice fed with normal water, the matrigel was filled with tumor cells (Figure 7H). The GFP shRNA-containing tumors did not respond to Dox treatment and continued to grow during the period of experiment.

DISCUSSION

ENTPD5 Is an Important Link in the PI3K/PTEN Signaling Loop

The experimental data reported here identify ENTPD5, an ER UDPase, as an important link in the PI3K/PTEN/AKT signaling loop. We reason that ENTPD5 upregulation is important for AKT-activated cells to cope with elevated translational activity that generates more nascent polypeptide chains destined for the ER.

ENTPD5 is a member of the ectonucleoside triphosphate diphosphohydrolase family, which consists of seven other members (reviewed by Robson et al., 2006). ENTPD 1–3 (CD39, CD39L1, and CD39L3) are typical ectoenzymes, whereas the other five members have a predominant intracellular localization including ER, Golgi apparatus, and lysosomal/autophagic vacuoles. The functions of these organelle-associated ENTPDases are still largely unexplored, but judging by their location and substrate preference, it would not be surprising if they all turn out to regulate protein glycosylation.

Among members of this group of enzymes, however, ENTPD5 is the only intracellular ENTPDase that is transcriptionally upregulated in PTEN null cells (Figure S1). The mRNA of an extracellular ENTPDase, ENTPD2, although expressed at a much lower level than ENTPD5, was also elevated in PTEN null cells (Figure S1). The significance of such is unknown.

ENTPD5 Contributes to Warburg Effect

One of the surprising findings reported here is how quickly ATP can be consumed as a result of ENTPD5 upregulation. One naturally raised question is where the extra consumed ATP comes from. After measuring both oxygen consumption and lactate generation, we found that the lactate production was elevated in these PTEN null cells, whereas oxygen consumption did not change (Figure 6A and Figure S4). When ENTPD5 was knocked down, higher lactate production returned to normal (Figure 6B). Moreover, simply ectopically expressing ENTPD5 in PTEN heterozygous MEF elevated their lactate production (Figure 6A). These results indicate that ENTPD5 is a critical player in causing the Warburg effect, i.e., elevated lactate production under aerobic conditions, in these PTEN null cells.

In addition to being part of the activation loop for AKT that promotes glucose uptake into cells (Kohn et al., 1996; Plas et al., 2001), a major effect of ENTPD5 on glycolysis might be its ability to generate ADP/AMP through the aid of CMPK1 and AK1. Elevated AMP levels (and to a lesser extent, ADP) activate phosphofructokinase and inhibit fructose diphosphatase to drive glycolysis and prevent gluconeogenesis, resulting in higher lactate production (Gevers and Krebs, 1966). Consistently, the fructose-1,6-bisphosphate level dropped to a much lower level than that of fructose-6-phosphate when the ENTPD5 in PTEN null cells was knocked down (Figure 6E).

In addition to UDP, ENTPD5 also use GDP as a substrate and hydrolyze it to GMP (Figure 3A and Figure S3). It is interesting to note that GDP-conjugated sugars are another group of major substrates for glycosylation. The significance of hydrolyzing GDP by ENTPD5 is not clear because it is believed that GDP sugars are transferred to proteins in the Golgi.

ENTPD5 Is Potentially an Anticancer Target

The current study highlighted ENTPD5 as a critical link in the PI3K/PTEN pathway that promotes cell growth and survival, a pathway that is often activated in cancer cells. We saw good correlation between ENTPD5 expression and AKT activation in both cultured prostate cancer cell lines and primary human prostate carcinoma samples (Figures 7A and 7B and Figures S6 and S7). Therefore, inhibition of this enzyme, similar to knockdown, can potentially generate benefits for anticancer activity. It should induce more severe ER stress in cancer cells with active AKT due to higher protein traffic through the secretory pathway. It may cause synthetic lethality in these cells, which otherwise maintain survival advantage and resistance to common anticancer drugs. It will also lower many growth factor receptors on the cell surface due to their high N-glycosylation nature, a phenomenon that may reflect the evolutionary connection between fast growth and nutrient availability in mammalian cells (Lau et al., 2007). Among such receptors, EGFR, Her2/ErB2, and IGFR levels were down after ENTPD5 knockdown (Figure 5 and Figure 7), whereas a nongrowth-promoting TGFβ receptor did not change (data not shown).

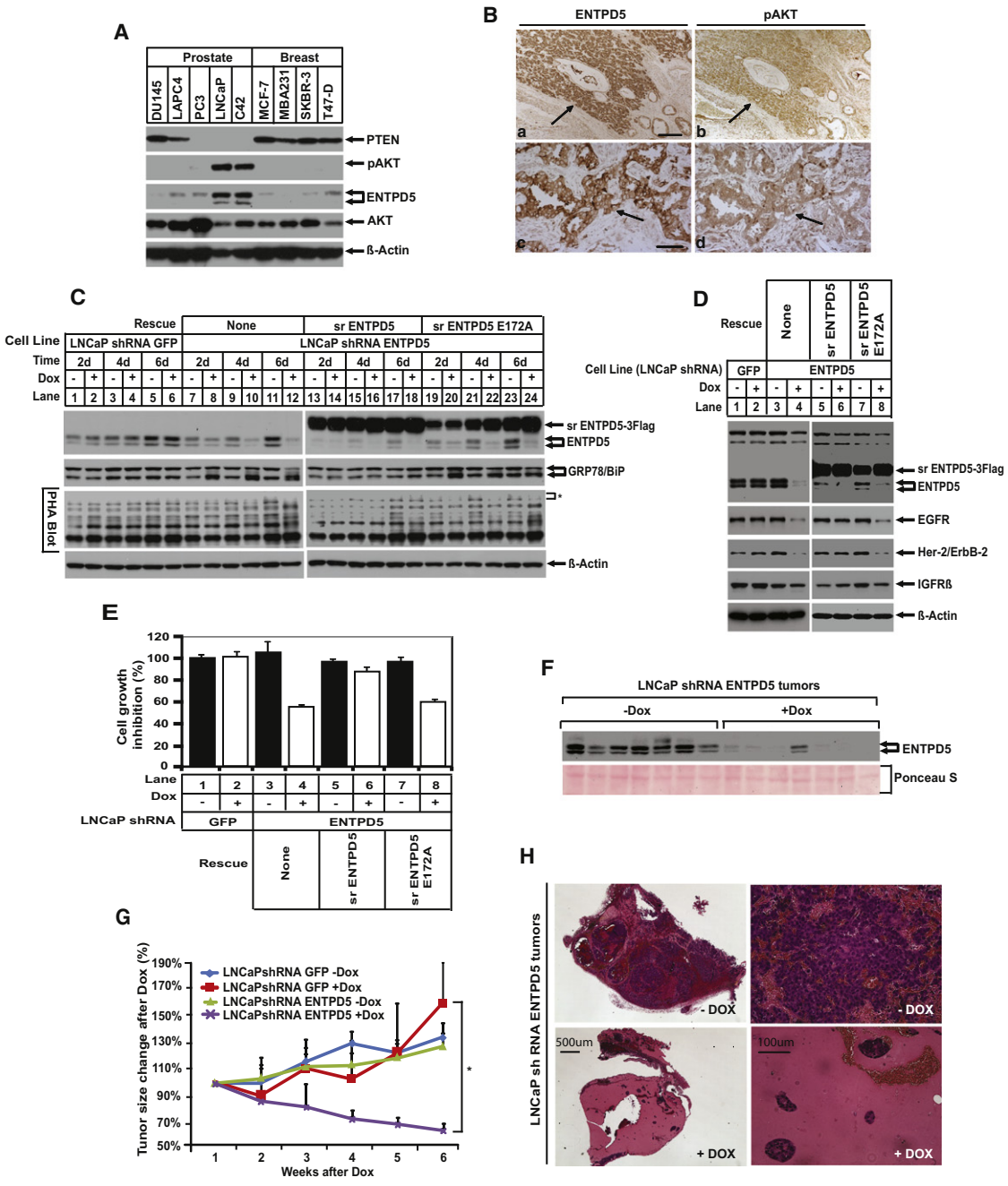

Figure 7. Knockdown of ENTPD5 in LNCaP Cells Decreases Glycosylation, Expression of Cell Surface Receptors, and Tumor Progression

(A) Aliquots of 20 μg of total cell extracts from indicated cell lines were subjected to 10% SDS-PAGE followed by western blotting analysis using antibodies as indicated.

(B) Immunohistochemical staining for ENTPD5 (a and c) and pAKT (b and d) in adjacent sections of a human prostatic carcinoma sample (a/b 10× and c/d 20× lenses). Scale bar, 200 μM (a and b); 100 μM (c and d). Arrows indicate tumor.

(C) Inducible ENTPD5 knockdown and rescue stable cell lines were treated with or without Dox (0.0625 μg/ml) for indicated time periods. Aliquots of 10 μg of total cell extracts were subjected to 10% SDS-PAGE for western blotting analysis of ENTPD5, BiP, glycosylated proteins (PHA blot), and β-actin. Asterisk indicates decreased glycosylated proteins.

(D) Indicated cell lines were plated and treated with or without Dox for 6 days, total cell lysates were prepared, and aliquots of 10 μg protein were subjected to SDS-PAGE followed by western blotting analysis using indicated antibodies.

(E) Indicated cells (1×10^4) were seeded in 96-well plates and then treated with and without Dox (1 μg/ml) for 4 days. Cell contents were measured.

(F–H) 2×10^6 LNCaP cells with Dox-inducible shRNA target GFP or ENTPD5 were injected subcutaneously into the flank of nude mice as described in the Extended Experimental Procedures. When the tumors reached a volume of ~500 mm^3, mice were fed with normal or Dox-containing water.

Chronic inhibition of ENTPD5 may cause liver and male fertility defects because mice with ENTPD5 deficiency show hepatopathy and aspermia (Read et al., 2009). These defects in mice, however, only become obvious after 1 year of age. Given the poor prognosis of PI3K/PTEN mutations in human cancers and potential synthetic lethal effect of AKT activation and ENTPD5 inhibition, developing ENTPD5 inhibitors for cancer therapy may be a worthwhile pursuit.

EXPERIMENTAL PROCEDURES

General Reagents and Methods

General chemicals are from Sigma unless otherwise described. We obtained α-P^{32}-labeled ATP from GE Healthcare. All other nucleotides are from Sigma. Nonhydrolyzable uracil and guanine nucleotide analogs are from Gena Bioscience (Germany). HRP-conjugated E-type PHA is from USBioLogical (Ca#P3371-25). Puromycin, blasticidin, and hygromycin, which are used for establishment and maintenance of stable cell lines, are purchased from Invivogen (Ca#ant-pr-1, ant-bl-1, and ant-hg-1, respectively). G418 is from Calbiochem (Ca#345810). The sources of antibodies used are listed in the Extended Experimental Procedures.

Cell Culture

PTEN$^{+/-}$ and *PTEN*$^{-/-}$ MEF cells are established previously (Stambolic et al., 1998). The sources of all other cell lines used and their culture conditions are described in the Extended Experimental Procedures.

In Vitro ATP Hydrolysis Assay

The ATP hydrolysis assays were carried out by incubation-indicated cell extracts or purified enzymes with α-P^{32}-ATP and were analyzed by thin layer chromatography (TLC). The detailed method was described in the Extended Experimental Procedures.

Purification of ENTPD5 and CMPK

All purification steps were carried out at 4°C. All chromatography steps were carried out using an automatic fast protein liquid chromatography (FPLC) station (Pharmacia). The details of purification methods were described in the Extended Experimental Procedures.

ENTPD5 Expression and ENTPD5 shRNA Constructs

All ENTPD5 expression and shRNA constructs were made as described in the Extended Experimental Procedures.

Preparation of Recombinant ENTPD5, CMPK1, and Adenylate Kinase

Human ENTPD5 recombinant protein was generated using Bac-to-Bac Baculovirus Expression Systems (Invitrogen Cat# 10359-016). Human CMPK1 and AK1 were generated by bacterial expression. The details of methods were described in the Extended Experimental Procedures.

Measurement of Lactate Production in Cell Culture Medium

We purchased Lactate Assay kit from Biovision (Cat#K627-100). Measurement of Lactate concentration in cell culture medium was performed according the manufacturer's instruction and described in detail in the Extended Experimental Procedures.

Measurement of Intracellular Fructose-6-P and Fructose-1,6-2P

The preparation and measurement of these two phosphosugars by LC-Mass were described in the Extended Experimental Procedures.

Cell Survival Assay

Cell survival analysis was performed using the Cell Titer-Glo Luminescent Cell Viability Assay kit (Promega) following manufacturer's instruction with minor modification. In brief, 25 μl of Cell Titer-Glo reagent was added to the cell culture medium. Cells were placed on a shaker for 10 min and were then incubated at room temperature for an additional 10 min. Luminescent reading was carried on a Tecan SPECTRAFluor Plus reader (Tecan).

SUPPLEMENTAL INFORMATION

Supplemental Information includes Extended Experimental Procedures, seven figures, and one table and can be found with this article online at doi:10.1016/j.cell.2010.10.010.

ACKNOWLEDGMENTS

We would like to express our gratitude to Drs. Fenghe Du and Liping Liu for excellent technical assistance. We are grateful for Dr. Aijun Liu from the 301 Hospital in Beijing for providing the human prostate tumor samples and Dr. Benjamin Tu from University of Texas Southwestern for help with the phosphofructose sugar measurement. We thank Mr. Gregory Kunkel and Dr. Lai Wang for critical reading of the manuscript. This work is also supported by a grant from the National Cancer Institute (NCI) (PO1 CA 95471) and the National High Technology Projects 863 from Chinese Ministry of Science and Technology.

Received: May 14, 2010
Revised: September 10, 2010
Accepted: October 7, 2010
Published online: November 11, 2010

REFERENCES

Bermudo, R., Abia, D., Ferrer, B., Nayach, I., Benguria, A., Zaballos, A., del Rey, J., Miró, R., Campo, E., Martínez-A, C., et al. (2008). Co-regulation analysis of closely linked genes identifies a highly recurrent gain on chromosome 17q25.3 in prostate cancer. BMC Cancer *8*, 315.

Brunet, A., Bonni, A., Zigmond, M.J., Lin, M.Z., Juo, P., Hu, L.S., Anderson, M.J., Arden, K.C., Blenis, J., and Greenberg, M.E. (1999). Akt promotes cell survival by phosphorylating and inhibiting a Forkhead transcription factor. Cell *96*, 857–868.

Christofk, H.R., Vander Heiden, M.G., Harris, M.H., Ramanathan, A., Gerszten, R.E., Wei, R., Fleming, M.D., Schreiber, S.L., and Cantley, L.C. (2008). The M2 splice isoform of pyruvate kinase is important for cancer metabolism and tumour growth. Nature *452*, 230–233.

Ellgaard, L., Molinari, M., and Helenius, A. (1999). Setting the standards: quality control in the secretory pathway. Science *286*, 1882–1888.

Elstrom, R.L., Bauer, D.E., Buzzai, M., Karnauskas, R., Harris, M.H., Plas, D.R., Zhuang, H., Cinalli, R.M., Alavi, A., Rudin, C.M., and Thompson, C.B. (2004). Akt stimulates aerobic glycolysis in cancer cells. Cancer Res. *64*, 3892–3899.

Engelman, J.A., Luo, J., and Cantley, L.C. (2006). The evolution of phosphatidylinositol 3-kinases as regulators of growth and metabolism. Nat. Rev. Genet. *7*, 606–619.

(F) Tumors lysates were extracted after 6 weeks, and aliquots of 20 μg of protein were subjected to 10% SDS-PAGE and transfer to nitrocellulose filter. The filter was stained with Ponceau S staining (bottom) followed by western blotting analysis using an antibody against ENTPD5 (top).
(G) Time course of tumor shrinkage caused by ENTPD5 knocking down. Tumor size was measured, and statistic analysis was performed as described in the Extended Experimental Procedures. Each group consisted of seven mice. The values are represented as mean ± SD. *$p < 0.05$.
(H) Hematoxylin and eosin staining of resected tumors. (Left) Scale bar, 500 um. (Right) Scale bar, 100 um. (Top) Tumor without Dox. (Bottom) Tumor with Dox. See also Figure S6 and Figure S7.

Fewell, S.W., Travers, K.J., Weissman, J.S., and Brodsky, J.L. (2001). The action of molecular chaperones in the early secretory pathway. Annu. Rev. Genet. *35*, 149–191.

Fingar, D.C., Salama, S., Tsou, C., Harlow, E., and Blenis, J. (2002). Mammalian cell size is controlled by mTOR and its downstream targets S6K1 and 4EBP1/eIF4E. Genes Dev. *16*, 1472–1487.

Franke, T.F., Kaplan, D.R., Cantley, L.C., and Toker, A. (1997). Direct regulation of the Akt proto-oncogene product by phosphatidylinositol-3,4-bisphosphate. Science *275*, 665–668.

Gevers, W., and Krebs, H.A. (1966). The effects of adenine nucleotides on carbohydrate metabolism in pigeon-liver homogenates. Biochem. J. *98*, 720–735.

Helenius, A., and Aebi, M. (2004). Roles of N-linked glycans in the endoplasmic reticulum. Annu. Rev. Biochem. *73*, 1019–1049.

Hirschberg, C.B., Robbins, P.W., and Abeijon, C. (1998). Transporters of nucleotide sugars, ATP, and nucleotide sulfate in the endoplasmic reticulum and Golgi apparatus. Annu. Rev. Biochem. *67*, 49–69.

Keniry, M., and Parsons, R. (2008). The role of PTEN signaling perturbations in cancer and in targeted therapy. Oncogene *27*, 5477–5485.

Kohn, A.D., Summers, S.A., Birnbaum, M.J., and Roth, R.A. (1996). Expression of a constitutively active Akt Ser/Thr kinase in 3T3-L1 adipocytes stimulates glucose uptake and glucose transporter 4 translocation. J. Biol. Chem. *271*, 31372–31378.

Lau, K.S., Partridge, E.A., Grigorian, A., Silvescu, C.I., Reinhold, V.N., Demetriou, M., and Dennis, J.W. (2007). Complex N-glycan number and degree of branching cooperate to regulate cell proliferation and differentiation. Cell *129*, 123–134.

Maehama, T., and Dixon, J.E. (1998). The tumor suppressor, PTEN/MMAC1, dephosphorylates the lipid second messenger, phosphatidylinositol 3,4,5-trisphosphate. J. Biol. Chem. *273*, 13375–13378.

Plas, D.R., Talapatra, S., Edinger, A.L., Rathmell, J.C., and Thompson, C.B. (2001). Akt and Bcl-xL promote growth factor-independent survival through distinct effects on mitochondrial physiology. J. Biol. Chem. *276*, 12041–12048.

Read, R., Hansen, G., Kramer, J., Finch, R., Li, L., and Vogel, P. (2009). Ectonucleoside triphosphate diphosphohydrolase type 5 (Entpd5)-deficient mice develop progressive hepatopathy, hepatocellular tumors, and spermatogenic arrest. Vet. Pathol. *46*, 491–504.

Robson, S.C., Sévigny, J., and Zimmermann, H. (2006). The E-NTPDase family of ectonucleotidases: Structure function relationships and pathophysiological significance. Purinergic Signal. *2*, 409–430.

Stambolic, V., Suzuki, A., de la Pompa, J.L., Brothers, G.M., Mirtsos, C., Sasaki, T., Ruland, J., Penninger, J.M., Siderovski, D.P., and Mak, T.W. (1998). Negative regulation of PKB/Akt-dependent cell survival by the tumor suppressor PTEN. Cell *95*, 29–39.

Stephens, L., Anderson, K., Stokoe, D., Erdjument-Bromage, H., Painter, G.F., Holmes, A.B., Gaffney, P.R.J., Reese, C.B., McCormick, F., Tempst, P., et al. (1998). Protein kinase B kinases that mediate phosphatidylinositol 3,4,5-trisphosphate-dependent activation of protein kinase B. Science *279*, 710–714.

Trombetta, E.S., and Helenius, A. (1999). Glycoprotein reglucosylation and nucleotide sugar utilization in the secretory pathway: identification of a nucleoside diphosphatase in the endoplasmic reticulum. EMBO J. *18*, 3282–3292.

Trombetta, E.S., and Parodi, A.J. (2003). Quality control and protein folding in the secretory pathway. Annu. Rev. Cell Dev. Biol. *19*, 649–676.

Vander Heiden, M.G., Cantley, L.C., and Thompson, C.B. (2009). Understanding the Warburg effect: the metabolic requirements of cell proliferation. Science *324*, 1029–1033.

Warburg, O. (1925). Uber den Stoffwechsel der Carcinomzelle. Klin. Wochenschr. *4*, 534–536.

Whitman, M., Downes, C.P., Keeler, M., Keller, T., and Cantley, L.C. (1988). Type I phosphatidylinositol kinase makes a novel inositol phospholipid, phosphatidylinositol-3-phosphate. Nature *332*, 644–646.

Yuan, T.L., and Cantley, L.C. (2008). PI3K pathway alterations in cancer: variations on a theme. Oncogene *27*, 5497–5510.